Total variation approach for adaptive nonuniformity correction in focal-plane arrays

Esteban Vera,[1,2,*] Pablo Meza,[1,2] and Sergio Torres[1,2]

[1]*Departmento de Ingeniería Eléctrica, Universidad de Concepción, Casilla 160-C, Concepción, Chile*

[2]*Center for Optics and Photonics, Universidad de Concepción, Casilla 4016, Concepción, Chile*

**Corresponding author: estebanvera@udec.cl*

Received August 10, 2010; revised November 9, 2010; accepted December 2, 2010;
posted December 6, 2010 (Doc. ID 133239); published January 10, 2011

In this Letter we propose an adaptive scene-based nonuniformity correction method for fixed-pattern noise removal in imaging arrays. It is based on the minimization of the total variation of the estimated irradiance, and the resulting function is optimized by an isotropic total variation approach making use of an alternating minimization strategy. The proposed method provides enhanced results when applied to a diverse set of real IR imagery, accurately estimating the nonunifomity parameters of each detector in the focal-plane array at a fast convergence rate, while also forming fewer ghosting artifacts. © 2011 Optical Society of America

OCIS codes: 110.3080, 110.4155, 110.4280.

Imaging detectors, such as focal-plane arrays (FPAs), suffer from an undesired fixed-pattern noise (FPN) owing to the nonuniform response of the individual detectors when stimulated by the same level of irradiance. This effect is stronger at longer wavelengths, such as in IRFPAs [1], producing a severe mitigation on the quality and the effective resolution of the imaging system [2]. Thus, nonuniformity correction (NUC) is a mandatory task for properly calibrating and using several FPA-based cameras.

At any given frame n, the FPN generative model for each $\{ij\}$ detector in the FPA is often described by a linear relationship between the incoming irradiance $X_{i,j}(n)$ and the readout data $Y_{i,j}(n)$ as follows:

$$Y_{i,j}(n) = A_{i,j}X_{i,j}(n) + B_{i,j} + V_{i,j}(n), \tag{1}$$

where $A_{i,j}$ and $B_{i,j}$ are the gain and offset parameters associated to each $\{ij\}$ detector, respectively, and $V_{i,j}(n)$ is an additive zero-mean Gaussian noise term due mostly to the readout electronics. As the spatial disparities of the gain and offset parameters are the responsible for the FPN, NUC is about estimating these parameters to calibrate the readout data in order to compute the true incoming irradiance. This can be done by measuring two different uniform sources with a procedure named two-point calibration [3]. Unfortunately, and depending on environmental and operational conditions, the parameters may drift over time, so a continuous calibration is required, but sources such as blackbody (BB) radiators for the IR are not readily available in all situations. In this case, scene-based NUC methods have been developed to avoid the need of calibration sources or halting normal camera operations, estimating the needed parameters from the readout imagery [4]. Such algorithms rely on the data diversity found in most of the video sequences with some degree of motion, and they have been successfully performed in a block of frames basis using statistical methods [5,6] and also by using image registration techniques [7]. On the other hand, special interest has also been focused in the development of adaptive algorithms that allow for real-time implementations in a frame-by-frame basis [8,9]. However, the main drawback of these adaptive NUC methods is related to the generation of ghosting artifacts, which is a different source of FPN triggered by a poor estimation of the nonuniform gain and offset parameters. Nevertheless, in the particular case of the neural network method [8] (NN-NUC), recent strategies for enhancing the estimation process have been analyzed in [10] and later summarized in the fast adaptive NUC method proposed in [11] (FA-NUC), yielding new degrees of spatial adaptiveness with improved results.

Based on its success in image denoising applications, the aim of this Letter is to present a new adaptive scene-based NUC method, TV-NUC, based on the minimization of the total variation (TV) [12] of the estimated irradiance $\hat{X}(n)$, where

$$\mathrm{TV}(\hat{X}(n)) = \|\hat{X}(n)\|_{\mathrm{TV}} = \sum_{i,j} |\nabla \hat{X}(n)|_{i,j}. \tag{2}$$

The optimization process for TV-NUC is developed in a frame-by-frame basis, being a natural extension of the former NN-NUC method, which could also be considered as equivalent to the minimization of a quadratic smoothness prior model (Tikhonov regularization). Hence, for any given frame n, the idea is to estimate the nonuniformity gain ($\hat{A}_{i,j}$) and offset ($\hat{B}_{i,j}$) parameters that minimize $\mathrm{TV}(\hat{X})$, subject to $Y_{i,j} - \hat{A}_{i,j}\hat{X}_{i,j} - \hat{B}_{i,j} = 0$, $\forall\{ij\}$. The associated gradient for calculating the TV-norm can be approximated by first-order differences in backward or forward directions as follows:

$$|\nabla \hat{X}|_{i,j} = \sqrt{(\hat{X}_{i,j} - \hat{X}_{i-1,j})^2 + (\hat{X}_{i,j} - \hat{X}_{i,j-1})^2}, \tag{3}$$

or

$$|\nabla^* \hat{X}|_{i,j} = \sqrt{(\hat{X}_{i,j} - \hat{X}_{i+1,j})^2 + (\hat{X}_{i,j} - \hat{X}_{i,j+1})^2}. \tag{4}$$

Considering that the true irradiance can be estimated by using the inverse of the generative model in Eq. (1), then NUC is achieved for any frame n by computing

$$\hat{X}_{i,j}(n) = \hat{G}_{i,j}(n)Y_{i,j}(n) + \hat{O}_{i,j}(n), \tag{5}$$

where $\hat{O}_{i,j}$ and $\hat{G}_{i,j}$ are the correcting parameters related to the estimation of the gain and offset, such as $\hat{A}_{i,j} = 1/\hat{G}_{i,j}$ and $\hat{B}_{i,j} = -\hat{O}_{i,j}/\hat{G}_{i,j}$. Now, if we minimize Eq. (2) with respect to $\hat{O}_{i,j}$ and $\hat{G}_{i,j}$, using a gradient descent strategy in a frame-by-frame basis, then by choosing either of the discrete gradient versions in Eq. (3) or Eq. (4), the correcting parameters can be updated as

$$\hat{G}_{i,j}(n+1) = \hat{G}_{i,j}(n) - \lambda_{\mathrm{TV}} \frac{\hat{X}_{i,j}(n) - T_{i,j}(n)}{|\nabla \hat{X}|_{i,j}} Y_{i,j}(n),$$
$$\hat{O}_{i,j}(n+1) = \hat{O}_{i,j}(n) - \lambda_{\mathrm{TV}} \frac{\hat{X}_{i,j}(n) - T_{i,j}(n)}{|\nabla \hat{X}|_{i,j}}, \quad (6)$$

or

$$\hat{G}_{i,j}(n+1) = \hat{G}_{i,j}(n) - \lambda_{\mathrm{TV}} \frac{\hat{X}_{i,j}(n) - T^{*}_{i,j}(n)}{|\nabla^{*} \hat{X}|_{i,j}} Y_{i,j}(n),$$
$$\hat{O}_{i,j}(n+1) = \hat{O}_{i,j}(n) - \lambda_{\mathrm{TV}} \frac{\hat{X}_{i,j}(n) - T^{*}_{i,j}(n)}{|\nabla^{*} \hat{X}|_{i,j}}, \quad (7)$$

respectively, where λ_{TV} is a positive constant, and both $T_{i,j}(n) = (1/3)(\hat{X}_{i,j}(n) + \hat{X}_{i-1,j}(n) + \hat{X}_{i,j-1}(n))$ or $T^{*}_{i,j}(n) = (1/3)(\hat{X}_{i,j}(n) + \hat{X}_{i+1,j}(n) + \hat{X}_{i,j+1}(n))$ are an average of selected neighbor pixels. Thereby, we obtain an adaptive algorithm for performing NUC first by updating the parameters using either Eq. (6) or Eq. (7) and then applying Eq. (5) to estimate the irradiance. Nevertheless, whenever it is applied to video sequences, artifacts arise due to an anisotropic diffusion effect when selecting any of the derived options. Although this anisotropic behavior is common, and also expected, in classical TV denoising applications of single images, it is undesired for the present frame-based adaptive NUC application in image sequences. Therefore, we now introduce an alternating minimization approach that makes use of both update equations derived from the respective versions of the discrete gradient. In this way, we use Eq. (6) for an odd frame n, and Eq. (7) for an even frame n, thus obtaining the proposed isotropic TV-based adaptive NUC algorithm: TV-NUC.

When inspecting the update formulas, TV-NUC has similarities to both the original NN-NUC and FA-NUC as well. First, all of the methods use a global step constant, or learning rate such as λ_{TV}, for controlling the gradient descent optimization process. Second, in all cases the numerator presents a difference, or error, between the actual estimation $\hat{X}_{i,j}(n)$ and a target value $T_{i,j}(n)$ composed of a local weighted average. And, finally, the discrete gradient that appears in the denominator has a reminiscence of the local spatial standard deviation computed in FA-NUC, aimed for controlling the update process independently for each pixel. But there is a key difference: instead of posing an explicit heuristic and *ad hoc* spatial adaptive learning rate formula, henceforth it is inherited in the TV-NUC minimization process.

Table 1. Mean ISNR (dB)/Roughness (ρ) Results

IR Data	08:00	09:30	11:00	13:00
NN-NUC	3.2/0.100	2.8/0.129	3.7/0.137	3.5/0.284
FA-NUC	3.8/0.095	3.2/0.123	3.9/0.137	4.1/0.165
TV-NUC	4.4/0.093	3.7/0.121	4.9/0.128	5.1/0.162

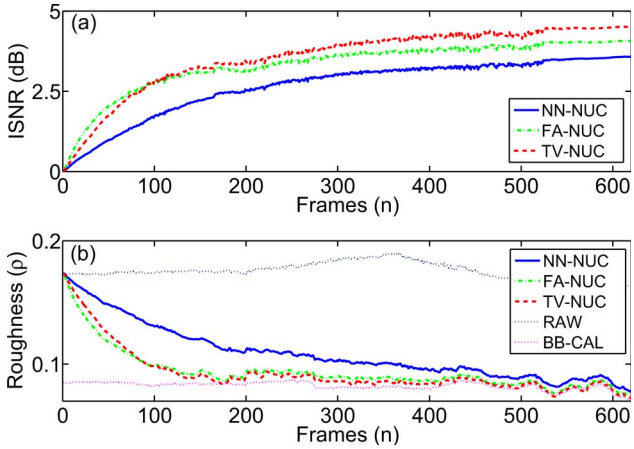

Fig. 1. (Color online) NUC performance on an SWIR video (08:00 a.m.): (a) ISNR (dB) and (b) roughness (ρ).

We contrast the performance of the proposed TV-NUC algorithm against NN-NUC (using a 3×3 spatial average kernel as suggested in [10]) and FA-NUC. We test the algorithms over a set of four 4000 frames real IR videos (RAW) captured by an Amber 4128 InSb camera (3–5 μm) at different times of the same day, ranging from 8 a.m. to 1 p.m. For each method, we perform an appropriate fine-tuning of the learning parameters, seeking the best performance while keeping a fair balance between speed and stability. Typically when testing NUC in real IR videos, and apart from the naked-eye evaluation, only a reference-free method such as the roughness index (ρ), which measures the high-pass content of an image, is often used [6,11]. However, because we also have a BB-calibrated version (BB-CAL) of the dataset, we can also calculate the associated improvement in signal-to-noise ratio (ISNR). Results for the averaged values obtained for each method and every test sequence are condensed in Table 1, where TV-NUC presents a consistent increase of around 20% in terms of the ISNR over FA-NUC, and at least 30% over NN-NUC. In addition, TV-NUC reports the smallest values of ρ.

As an example, the NUC evolution for the first 600 frames of the 8 a.m. sequence is displayed in Fig. 1. The ISNR for TV-NUC grows as fast as FA-NUC for the first 200 frames, but then it keeps increasing, reaching a gap of nearly 0.6 dB over FA-NUC, and 1.4 dB over NN-NUC, which is consistent to the mean values reported in

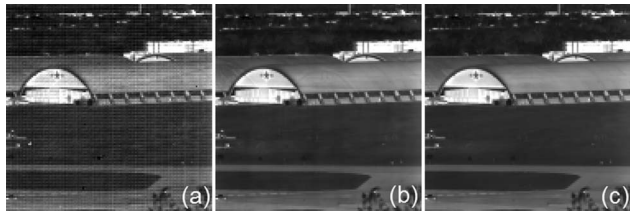

Fig. 2. (Media 2) Sample of NUC on an SWIR video (09:30 a.m.): (a) RAW frame 500: PSNR = 28.8 dB/ρ = 0.206, (b) NN-NUC: PSNR = 32.2 dB/ρ = 0.118, and (c) TV-NUC: PSNR = 33.1 dB/ρ = 0.114.

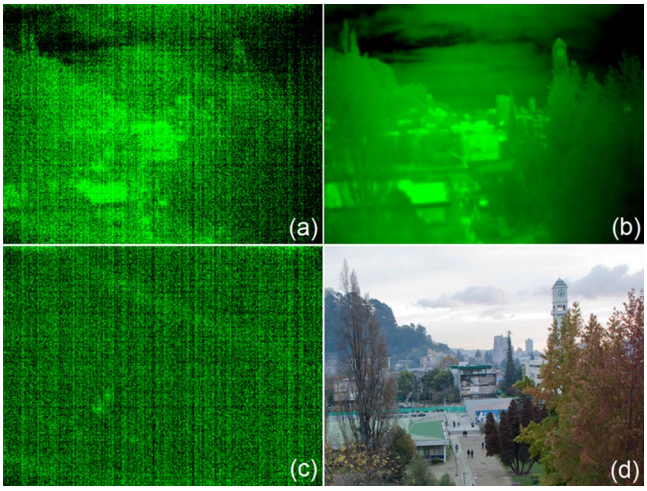

Fig. 3. (Color online) (Media 6) Sample of NUC on an LWIR video: (a) RAW frame 600: $\rho = 0.040$, (b) TV-NUC: $\rho = 0.009$, (c) estimated offset, and (d) visible image.

Table. 1. This gap is maintained throughout the rest of the sequence, and a similar behavior is also observed from the plots for the remaining test videos. From Fig. 1(b) we can realize that FA-NUC and TV-NUC required only less than 250 frames to closely track the ρ level of the clean images (BB-CAL), while NN-NUC needed almost double. Therefore, we may conclude that both FA-NUC and TV-NUC have a similar, and also better, NUC performance than NN-NUC, but after checking Fig. 1(a), we are confident that TV-NUC is even more accurate.

Companion movies comparing NN-NUC and TV-NUC in real-time are presented in Media 1, Media 2, Media 3, Media 4, and Media 5, corresponding to 500 frames of 8:00, 9:30, 11:00, 13:00, and an unknown time InSb IR image sequences, respectively. After a naked-eye evaluation, the ability of TV-NUC for compensating for the FPN promptly is clearly seen. Although some ghosting artifacts may be perceived in both cases, we can corroborate that they are quickly removed in TV-NUC. An image sample of this situation is presented in Fig. 2 (Media 2), where even if both NUC algorithms have already been able to significantly reduce the FPN, NN-NUC presents clear signs of a persistent ghosting trace from a previous frame.

We also captured IR data using a Cedip JADE-UC uncooled microbolometer camera (8–12 μm). The generated movies comparing the RAW and TV-NUC videos are presented in Media 6, Media 7, and Media 8, where again we notice the dexterity of TV-NUC for quickly cleaning the videos. A sample frame is depicted in Figs. 3(a) and 3(b) (Media 6), where the TV-NUC image in Fig. 3(b) shows no signs of FPN when compared to the visible image in Fig. 3(d), while the estimated offset in Fig. 3(c) apparently gathered the pure FPN. Accordingly, by using TV-NUC we are able to calibrate this camera with 10 s of video (600 frames at 60 Hz).

In summary, an adaptive scene-based NUC method for FPA is presented. It is based on the minimization of the TV of the estimated irradiance using a novel isotropic approach in a frame-by-frame basis. TV-NUC can be understood as a generalization of former adaptive NUC methods based on neural networks. The presented experiments with real IRFPA imagery demonstrated that TV-NUC not only surpasses other NUC techniques in terms of parameter estimation accuracy and convergence speed but also tends to form less ghosting artifacts even under strong FPN. Finally, we envisage that TV-NUC may be accelerated by knowing the FPA architecture [13], while ghosting may also be further reduced by using a gating strategy [14].

The authors thank E. Armstrong (OptiMetrics, Inc.) and the United States Air Force Research Laboratory (USAFRL, Dayton, Ohio) for providing the IR data (Amber). This work was supported by Programa de Financiamiento Basal grant PFB08024, Fondo Nacional de Desarrollo Científico y Tecnológico (FONDECYT 1100522), and CONICYT.

References

1. G. C. Holst, *Electro-Optical Imaging System Performance*, 5th ed. (SPIE Press, 2008).
2. A. Milton, F. Barone, and M. Kruer, Opt. Eng. **24**, 855 (1985).
3. D. Perry and E. Dereniak, Opt. Eng. **32**, 1854 (1993).
4. P. Narendra, Proc. SPIE **252**, 10 (1980).
5. P. Narendra and N. Foss, Proc. SPIE **282**, 44 (1981).
6. S. Torres and M. Hayat, J. Opt. Soc. Am. A **20**, 470 (2003).
7. B. Ratliff, M. Hayat, and J. Tyo, J. Opt. Soc. Am. A **22**, 239 (2005).
8. D. Scribner, K. Sarkady, M. Kruer, J. Caulfield, J. Hunt, M. Colbert, and M. Descour, Proc. SPIE **1541**, 100 (1991).
9. J. Harris and Y. Chiang, Proc. SPIE **3061**, 895 (1997).
10. S. Torres, E. Vera, R. Reeves, and S. Sobarzo, Proc. SPIE **5076**, 130 (2003).
11. E. Vera and S. Torres, EURASIP J. Appl. Signal Process. **2005**, 1994 (2005).
12. L. Rudin, S. Osher, and E. Fatemi, Physica D (Amsterdam) **60**, 259 (1992).
13. B. Narayanan, R. Hardie, and R. Muse, Appl. Opt. **44**, 3482 (2005).
14. R. Hardie, F. Baxley, B. Brys, and P. Hytla, Opt. Express **17**, 14918 (2009).